

## Treatment of organic pollutants in water using TiO<sub>2</sub> powders: photocatalysis versus sonocatalysis

Ivana Grčić · Dinko Vujević · Krunoslav Žižek ·  
Natalija Koprivanac

Received: 20 December 2012 / Accepted: 26 March 2013 / Published online: 12 April 2013  
© Akadémiai Kiadó, Budapest, Hungary 2013

**Abstract** The scope of this work was to explore the application of different TiO<sub>2</sub> powders (P25, PC105, PC500 and their calcined forms) for the photocatalytic and sonocatalytic treatment of model wastewaters containing single pollutants and their mixtures; dyes: C.I. Reactive Violet 2 (RV2), C.I. Mordant Yellow 10 (MY10) and oxalic acid. The influence of the applied catalyst type on the photocatalytic and sonocatalytic efficiency was explored with the emphasis on crystalline form and granulometric properties of powders. Generally, TiO<sub>2</sub> powders, which were applied as obtained, demonstrated higher photocatalytic activity (~20 % of organic content oxidized in the mixture of dyes and oxalic acid in 30 min) while their calcined forms were shown to be more prominent as sonocatalysts (up to 13 % of organic contents oxidized in 30 min). The XRD analysis of calcined TiO<sub>2</sub> powders confirmed the predominant crystal form of rutile. The degradation and mineralization kinetics of dyes RV2, MY10, oxalic acid and their mixtures was studied. In general, experimental results fitted well ( $R^2 > 0.94$ ) to the half and first order reaction rate model, pointing at the two ongoing mechanisms, i.e. reaction with ·OH radicals and direct electron transfer between adsorbed molecules and catalyst surface. A certain deviation is observed for the model solution containing dye MY10. MY10 serve as a filter for the UV-A irradiation ( $\lambda_{\text{max}} = 365$  nm). A detailed kinetic study confirmed the two simultaneous kinetic pathways and the comparable mechanisms for oxalic acid and dyes photocatalysis. The performed study confirmed the similarity of occurring mechanisms in photocatalysis and sonocatalysis due to sonoluminescence, with the extent of acoustic cavitation in ·OH radical generation.

---

I. Grčić (✉) · K. Žižek · N. Koprivanac  
Faculty of Chemical Engineering and Technology, University of Zagreb, Marulićev trg 19,  
HR-10000 Zagreb, Croatia  
e-mail: igrcic@fkit.hr

D. Vujević  
Department of Environmental Engineering, Faculty of Geotechnical Engineering, University of  
Zagreb, Hallerova aleja 7, HR-42000 Varaždin, Croatia

**Keywords** Photocatalysis · Sonocatalysis · Granulometric properties · Dye wastewaters · Kinetic study

### List of variables

$d$	Particle size (expressed with diameter value) (m)
$d_i$	Particle size in size class $i$ (m)
$\bar{d}_i$	Average particle size in size class $i$ (m)
$d_{3,2}$	Sauter mean diameter (m)
$d_p$	Pore size (expressed with diameter value) (m)
$d_{p,av.}$	Average pore size (expressed with diameter value) (m)
$dQ_3(d_i)$	Experimental data for volume content of entities in size interval $i$ (–)
$q_3(d)$	Normalized volume probability density function ( $m^{-1}$ )
$V$	Volume of adsorbed nitrogen gas that is pore volume ( $m^3$ )
$V_P$	Single point total pore volume ( $m^3 g^{-1}$ )
$S_V$	Estimated external surface area ( $m^2 m^{-3}$ )
$S_{BET}$	BET surface area ( $m^2 g^{-1}$ )
$\psi_{Wa}$	Wadel shape factor (–)
$i$	Discussed size interval ( $i = 1 \dots 86$ )
$r$	Reaction rate, $mol dm^{-3} s^{-1}$
$k$	Reaction rate constant, $mol^{1-n} dm^{3n-3} s^{-1}$
$n$	Reaction order
$X$	Extent, %
[.]	Molar concentration, $mol dm^{-3}$
$e_a$	Volumetric rate of photon absorption
$\theta$	Surface coverage
<b>a</b>	Coefficient for calculation of surface coverage at $t = 0$
<b>b</b>	Coefficient for calculation of changes in surface coverage
$a_k$	Exponential decay coefficient for reaction rate constants ( $s^{-1}$ )
$\lambda$	Wavelength, nm
$\lambda_{max}$	Wavelength of maxima absorption
$f$	Ultrasonic frequency, kHz
UV-A	Ultraviolet irradiation with maximum at 365 nm
UV-C	Ultraviolet irradiation with maximum at 254 nm

### Introduction

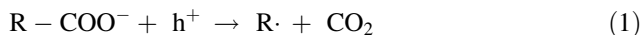
Purification of wastewater presents a significant role in the process of setting up water resources in the function of improving quality of life and economic growth, and concern for the human health protection and preservation of solid ecological conditions of water resources and environment in general. Specifically, wastewaters from dye manufacturing and the textile industry are characterized with the presence of different intermediates of complex structures and heavy metals, so such wastewaters are toxic and usually not suitable for purification by conventional

methods [1–4]. Due to the potential toxicity of dyes and corresponding intermediates and their visibility in surface waters, the removal and degradation of organic dyes have been a matter of considerable interest. On the other hand, a great number of aliphatic acids could be found in both wastewaters and natural waters. Oxalic acid appeared during the last step of mineralization of aromatic compounds [5, 6]. Moreover, it is known that oxalic acid is poorly degradable by hydroxyl radicals ( $\cdot\text{OH}$ ) radicals. Namely, the reaction rate constant between oxalic acid and the  $\cdot\text{OH}$  radical is approximately two orders of magnitude lower than the reaction rate constant between other organics and  $\cdot\text{OH}$  radical [7].

Heterogeneous photocatalysis is based on certain optical properties of semi-conducting materials. The concept of photocatalytic degradation is simple: an electron/hole pair is generated in a semiconductor particle if a photon with appropriate energy is absorbed ( $\lambda < 380$  nm—the corresponding bandgap energy is  $>3.2$  eV). If these charge carriers reach the catalyst surface before recombination, they can be used for chemical reactions, i.e., for oxidation or reduction of pollutants. Furthermore,  $\cdot\text{OH}$  radicals and superoxide anions ( $\text{O}_2^{\cdot-}$ ) are generated due to the high recombination ratio of photoinduced electrons ( $e^-$ ) and holes ( $h^+$ ) in contact with water and oxygen. These radicals are strong oxidants. Hydroxyl radicals are able to oxidize different organic components at low concentrations [8–10]. Commonly used photocatalysts are pure or doped metal oxide semiconductors, including the application of  $\text{TiO}_2$  in anatase or rutile form. Certain drawbacks divulged from semiconductor photocatalysis can be minimized by adopting the sonocatalytic degradation; especially for the treatment of semi- and low-transparent organic wastewaters. Due to the large numbers of aromatic compounds present in many dye molecules and stability of modern dye, sometimes the conventional photocatalytic degradation methods are ineffective for decolorization and mineralization [11].

Sonochemical degradation of pollutants in water appeared as an attractive advanced oxidation technology. The addition of soluble and insoluble reagents to an ultrasonic reactor promotes the formation of cavities and generation of free radicals [12]. The use of insoluble particles (heterogeneous catalysis) such as metallic oxides (e.g.  $\text{TiO}_2$ ) and mixtures of metals is even more promising in accelerating sonochemical reactions [11–14]. Some studies reported efficient decolorization of dye model wastewater using ultrasound and  $\text{TiO}_2$  [15–18]. The sonocatalytic effect is based on the synergy of ultrasound and surface chemistry, i.e. enhancement of the oxidative power of ultrasound by increased surface area of the catalyst, and the formation of  $\cdot\text{OH}$  on metal surfaces by heterogeneous nucleation of the bubbles. Recent observations have indicated that  $\text{TiO}_2$  particles can enhance the oxidizing power of ultrasound even in the absence of ultraviolet irradiation [14]. It is known that the flushes of single bubble sonoluminescence involve intense ultraviolet light, and sonoluminescence caused by bubble/cavity implosion may induce the excitation of  $\text{TiO}_2$  in the ultrasonic system. Past studies indicated that the activation of the  $\text{TiO}_2$  photocatalyst by sonoluminescence caused a significant decomposition of phenolic compounds [19]. These observations may propose the possibility that ultrasonic irradiation over a  $\text{TiO}_2$  catalyst enhances the generation of  $\cdot\text{OH}$ , and this effect is mediated by mechanisms similar to those of  $\text{TiO}_2$  photocatalysis.

The key step in semiconductor catalysis involves the generation of the hole-electron pairs in the catalyst ( $\text{TiO}_2$  particle), which migrate to the surface, thus giving place to a competition between their recombination versus the interfacial charge transfer to the adsorbed species. It is undetermined whether the oxidation process proceeds via  $\cdot\text{OH}$  radicals generated upon hole trapping by  $\text{OH}^-$  or adsorbed water molecules or by direct hole transfer ( $h^+$ ) to an adsorbed pollutant, i.e. photo-Kolbe reaction mechanism, Eq. 1:



Some studies pointed out the preferred  $\cdot\text{OH}$ -attack route for the photodegradation of aromatic compounds, especially halogenated ones, while the photodegradation of aliphatic acids favors the  $h^+$  trapping path [20, 21]. Recently, the overall reaction rate of oxalic acid photodegradation was described as a combination of two pathways working in parallel. The latter resulted in the observation of two kinetic regimes: a faster first order kinetics associated with hole trapping via  $\text{OH}^-$  and a slower square root dependence of oxalic acid concentration due to direct hole trapping by the adsorbed species (half-order kinetics) [5, 22].

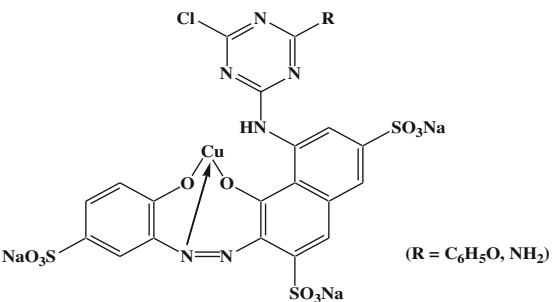
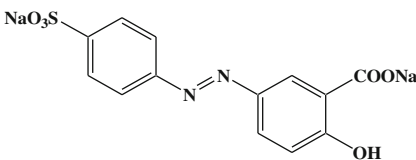
The goal of the study was to explore the applicability of given catalytic materials in terms of appropriate surface area, crystalline forms and high catalytic activity. In this study, we investigated the photocatalytic and sonocatalytic potential of three different commercially available  $\text{TiO}_2$  powders; P25 by Evonik, PC105 and PC500 by Millenium. In addition, the powders were calcined at  $915^\circ\text{C}$  to obtain the rutile form. The general idea was to show the preferred application of calcined  $\text{TiO}_2$  as a sonocatalyst, since it is known that rutile is more thermodynamically stable [18, 23]. Indeed, the performed study confirmed the higher efficiency of sonocatalysis with calcined  $\text{TiO}_2$ , while commercial (mostly anatase)  $\text{TiO}_2$  was confirmed to be more efficient for photocatalysis. The other objective of the study was to clarify the preferred degradation mechanism of organic compounds. Dyes and oxalic acid were chosen as pollutants because of the presumed different degradation mechanisms. However, according to the observed kinetics it was shown that all three pollutants undergo both reaction with  $\cdot\text{OH}$  radicals (first order kinetics) and hole trapping mechanism (half-order kinetics), thus pointing at different surface complexes pollutant- $\text{TiO}_2$ .

## Experimental

### Materials and catalyst preparation

The following chemicals were used in this study as received from the manufacturer: oxalic acid (HPLC grade, Aldrich), C.I. Reactive Violet 2 (RV2) and C.I. Mordant Yellow 10 (MY10) (CIBA Limited, Switzerland). Distilled water was used throughout this study. Spectral data and structural representations of the dyes selected for the present work are shown in Table 1. Six different model solutions were prepared; single pollutant model solutions: RV2, MY10, oxalic acid, and dye-acid mixtures: DAW1 (RV2 + oxalic acid), DAW2 (MY10 + oxalic acid) and

**Table 1** Structural representation of selected dyes

Dye	Structure	Molar extinction coefficient, (cm <sup>-1</sup> L mol <sup>-1</sup> )		
		254 nm	365 nm	550 nm
RV2		16,390	490	18,100
MY10		3,306	14,400	0

DAW3 (all three model pollutants). Note that the respective concentration of each pollutant was 50 mg L<sup>-1</sup>.

Different types of commercial and calcined TiO<sub>2</sub> powders, namely, P25 (Evonik), PC105 and PC500 (Cristal Global—Millenium) were used as the photocatalyst and sonocatalyst specimens for degradation of oxalic acid, MY10, RV2 and their mixtures.

The types of TiO<sub>2</sub> catalysts that have been used in this study are mostly in crystal form of anatase (Table 2). The anatase TiO<sub>2</sub> catalyst is more active in photocatalytic processes so it is necessary to subject them to thermal treatment in order to increase the percent of the rutile form, which is reportedly more active in sonocatalytic processes. Each TiO<sub>2</sub> powder was weighed and thermally treated in the oven. Heating of the catalyst was performed in temperature range from the room temperature up to 500 °C, which has been followed by heating to 915 °C with heating rate 1 °C/min.

#### Photocatalytic, sonocatalytic and additional experiments

Photocatalytic studies were performed in the glass water-jacketed batch reactor equipped with a quartz tube in middle for insertion of a low-pressure mercury lamp [24]. Two sources of UV irradiation with the radiant power ~ 5.4 W were used in the study: UV-C emitting irradiation with a maximum at 254 nm and UV-A emitting irradiation with a maximum at 365 nm (UVP Products, UK). The total volume of treated solutions was 0.5 L, while the mixing was provided by a magnetic stirring bar. The temperature was maintained at 22.0 ± 1.5 °C by circulating cooling water through the jacket of the

**Table 2** Granulometric and crystalline properties of used catalytic material

	Term	P25	PC-105	PC-500
Raw powder	Primary particle size, (nm)	20	15–25	5–10
	Crystalline form	Anatase:rutile = 75:25	Anatase	Anatase (>95 %)
	$S_v$ , ( $m^2 m^{-3}$ )	3,162,395	4,623,982	3,607,997
	$S_{BET}$ , ( $m^2 g^{-1}$ )	56.00	89.63	340.50
	$d_{3,2}$ , ( $\mu m$ )	2.65	1.72	2.02
	$d_{50}$ , ( $\mu m$ )	3.02	2.24	2.66
	$d_{modal}$ , ( $\mu m$ )	3.65	2.93	2.93
	$d_p$ , (nm)	10.49	14.92	6.71
After calcination at 915 °C	Crystalline form	Rutile	Anatase + rutile	Anatase + rutile
	$S_v$ , ( $m^2 m^{-3}$ )	32,015	55,571	506,220
	$S_{BET}$ , ( $m^2 g^{-1}$ )	3.97	5.59	4.56
	$d_{3,2}$ , ( $\mu m$ )	649.81	421.89	37.12
	$d_{50}$ , ( $\mu m$ )	906.39	602.55	75.66
	$d_{modal}$ , ( $\mu m$ )	1114.52	717.73	79.49
	$d_p$ , (nm)	7.64	8.60	7.80

photo-reactor. Sonocatalytic reaction studies were performed using an ultrasonic bath (Sonorex RK-510H, Bandelin, Germany; 320 W per transducer, 35 kHz). A reaction vessel of defined geometry (0.4 L, 7 cm in diameter) was placed directly above the transducer (5.4 cm in diameter). Additionally, the horn of an ultrasonic homogenizer (Sonopuls HD3200, Bandelin; 200 W, 20 kHz) was immersed in the center of the reaction mixture. In the given manner, an ultrasonic system with two frequencies was obtained. Sonication was employed individually or simultaneously. The temperature was maintained at  $28.0 \pm 2.5$  °C by circulating cooling water in ice-cooled ultrasonic bath.

Prior to experiments, the initial pH of the system was adjusted using a pH meter (Handylab pH/LF, Schott Instruments) at pH 4.0. An amount of  $1 g L^{-1}$  of corresponding  $TiO_2$  powder [25] was dispersed in the model solution and stirred in dark and silence for 30 min. All experiments were performed in a dark box to prevent the influence of daily or ambient light.

Additionally, in order to explore the effect of sonication on the granulometric properties of  $TiO_2$  powders (anatase), aqueous suspensions of commercial catalysts were sonicated for 20 min at different frequencies: 20, 35 and 20 + 35 kHz; with continuous sonication and pulse setup at  $f = 20$  kHz (1 s sonication + 5 s relaxation period). The suspension was then filtered through cellulose filters (0.2  $\mu m$ ), the solid resin was dried and subjected to further analysis.

## Analyses

The mineralization extents were determined on the basis of total organic carbon (TOC) content measurements, performed by using a TOC analyzer; TOC-V<sub>C<sub>PN</sub></sub> 5000 A, Shimadzu. A Perkin Elmer Lambda EZ 201 UV–Vis spectrophotometer

was used for monitoring decolorization at two different wavelengths, i.e.  $\lambda = 365$  and 550 nm, which correspond to the absorption maxima of MY10 and RV2. The concentration of each dye was determined on the basis of UV–Vis absorption at  $\lambda_{\max}$ , by applying the Lambert–Beer equation to the measured absorbances at their respective  $\lambda_{\max}$ . The concentrations of oxalic and other carboxylic acids were determined according to the procedure described in previous publications [6, 26].

For the XRD analysis of TiO<sub>2</sub> powders, a Bruker D8 diffractometer using Bragg–Brentano geometry and Cu K<sub>α</sub> wavelength ( $\lambda = 1.5418 \text{ \AA}$ ) in the  $5^\circ < 2\theta < 90^\circ$  range was used. Main diffraction peak positions were used to identify crystalline anatase and rutile polymorphic varieties.

The BET surface areas, pore volumes and pore size distribution were estimated from nitrogen adsorption and desorption isotherm data using an ASAP 2000 apparatus (Micromeritics Corporation). Prior to analysis, samples were degassed (6.6 Pa) at 400 °C to remove any physically adsorbed gases. The pore size distributions of the samples were determined by the BJH (Barret–Joyner–Halenda) model from the data of adsorption and desorption branch of the nitrogen isotherms.

Particle size distributions (PSDs) of photocatalytic samples were determined in wet mode applying the laser diffraction method (SALD 3101, Shimadzu, Japan). They are expressed, on the volume basis, with characteristic diameter mean values,  $d_{3,2}$  and reported via normalized volume density function,  $q_3(d)$ . The additional perspective of experimental PSDs is provided by estimation of specific surface area parameter. External specific surface area of a group of TiO<sub>2</sub> entities was estimated on the volume basis of experimental PSDs using Eq. 2.

$$S_V = \frac{6}{\psi_{wa}} \sum_{i=1}^{86} \frac{dQ_3(d_i)}{\bar{d}_i} \quad (2)$$

In this work, the estimation procedure integrates the assumption that each entity is a sphere.

## Results and discussion

### Relationship between catalytic efficiency and properties of TiO<sub>2</sub> powders

In order to determine the catalytic efficiency of different TiO<sub>2</sub> powders for the mineralization and degradation of model pollutants, the set of experiments, which included the application of UV irradiation or ultrasound in slurry, have been performed. The results are shown in Fig. 1. After both 30 and 60 min of treatment, the highest mineralization extent was achieved by applying the photocatalytic treatment (UV-A irradiation) of mixture DAW3 using commercial PC500 powder. Generally, PC500 used as obtained, showed the highest photocatalytic activity in terms of pollutant degradation (comparison data not shown). Note that PC500 possess the highest  $S_{\text{BET}}$  among investigated catalysts. Concerning sonocatalysis, almost the same mineralization extents were observed for all the calcined catalysts, while P25, used as obtained (raw), showed a higher efficiency than commercial

PC105 and PC500. The observed results indicate the higher efficiency of rutile in ultrasonic processes and confirm the known higher efficiency of anatase in photocatalysis. Moreover, rutile efficiency in photocatalysis is considerably lower than the efficiency observed using anatase.

As it can be seen (Fig. 2), calcined catalysts consist of both rutile and anatase phase, with the absence of brookite. Since raw P25 is 75–25% anatase over rutile (Table 2), calcination contributed to the complete transformation of anatase into more thermodynamically stable rutile. Calcination of raw powders contributed to transformation into rutile, but also to an increase in particle size and a consequent significant decrease of estimated total external surface area ( $S_V$ , Table 3). The decrease of  $S_V$  might cause a lack of photocatalytic activity of calcined  $\text{TiO}_2$  powders. Note that the  $\text{TiO}_2$  particle size is actually a size of  $\text{TiO}_2$  spheres/aggregates. It is different from a size of a single particle which is considered as nanosized according to manufacturers' data (Table 2). Moreover,  $S_{\text{BET}}$  values and the corresponding pore diameters also decrease significantly after the calcination of powders (Table 2).

The preferred sonocatalytic activity of rutile  $\text{TiO}_2$  over anatase  $\text{TiO}_2$  powder was also reported elsewhere [18]. Rutile  $\text{TiO}_2$  particles possess a suitable size with high sonocatalytic activity (as shown in Table 2; Fig. 1.), while anatase  $\text{TiO}_2$  particle can be destroyed to a certain extent. To estimate the effect of ultrasound on the size and surface of anatase  $\text{TiO}_2$  particles, an aqueous suspension of raw powders was sonicated in different modes for 20 min (as described in “Photocatalytic and sonocatalytic experiments” section). As given in Table 3 and Fig. 3, sonication influenced the certain granulometric properties of raw powders. According to the data given for P25 and PC105, the PSD of raw powders can be considered as bimodal with the estimated Sauter mean diameters ( $d_{3,2}$ ) of 2.650 and 1.717  $\mu\text{m}$  for P25 and PC105, respectively. Upon sonication of P25 suspensions, these diameters attain higher values, from 3.120 to 5.366  $\mu\text{m}$ . According to the obtained results, it

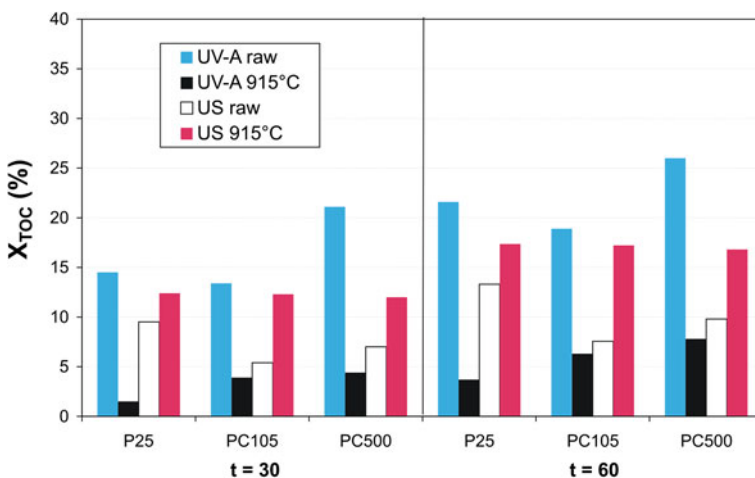


**Fig. 1** Mineralization extents observed after 30 and 60 min of applied processes in respect to the catalyst



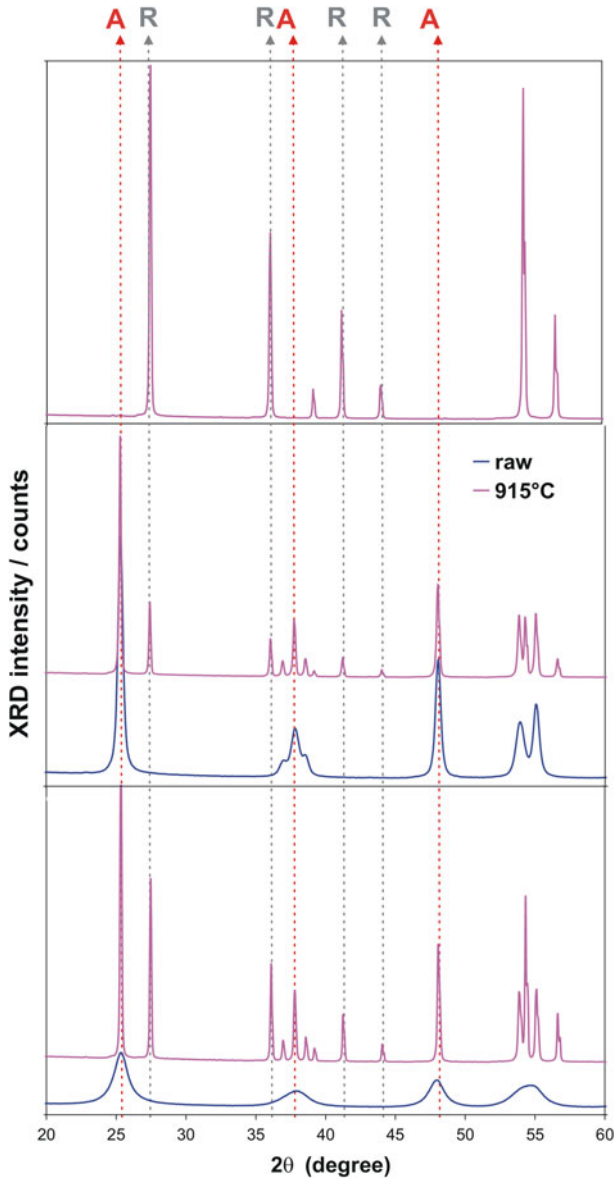


**Fig. 2** Results of XRD analysis for raw and calcined  $\text{TiO}_2$  powders; peaks marked with A and R correspond to anatase and rutile crystalline form, respectively

can be said that sonication excels the aggregation of  $\text{TiO}_2$  P25 particles, which follows the similar trend in the case of continuous sonication at 35 kHz (Table 3), while the aggregation is more enhanced during continuous sonication at 20 kHz. In all cases, two distinct fractions are detected (Fig. 3a): particles of  $\sim 1 \mu\text{m}$  (narrow distribution), and particles with larger diameter (broad distribution). The observed

**Table 3** PSD report; Sauter mean diameter values and estimated surface area for different TiO<sub>2</sub> samples after 20 min of sonication

Powder type	Term	Frequency, (kHz)				
		20	20 (pulse)	35	20 + 35	20 (pulse) + 35
P25	$S_v, (m^2 m^{-3})$	$2.055 \times 10^6$	$3.970 \times 10^6$	$3.387 \times 10^6$	$5.194 \times 10^6$	$3.192 \times 10^6$
	$d_{3,2}, (\mu m)$	5.366	3.120	4.212	4.030	4.294
PC-105	$S_v, (m^2 m^{-3})$	$5.085 \times 10^6$	$1.331 \times 10^6$	$4.478 \times 10^6$	$4.024 \times 10^6$	$6.778 \times 10^6$
	$d_{3,2}, (\mu m)$	2.058	6.409	1.544	1.903	1.057

broad distribution of particles with larger diameter (up to 10  $\mu m$ ) indicates the irregularity in aggregation of certain portion of TiO<sub>2</sub> entities. In the case of the PC105 suspension, its behavior during sonication is erratic and a repeatable trend cannot be observed (Fig. 3b). Estimated values of  $d_{3,2}$  also vary significantly from 1.057 to 6.409  $\mu m$ . In general, the comparative analysis of PSD in sonicated P25 and PC105 suspensions showed the seemingly uncertain behavior of PC105 particles. These observations favor the postulated theory of negative influence of ultrasound on anatase TiO<sub>2</sub> [18].

The surface area of a powder can critically affect its catalytic activity. Therefore, the next step was to quantify the changes in pore volume, pore size distribution and specific surface area of selected powders upon sonication (Fig. 3c, d). Sonication of the P25 suspension influenced the increase in the corresponding  $d_p$  and  $S_{BET}$  values ( $\sim 30\%$  increase), while sonication of the PC105 suspension caused the 60% increase in  $S_{BET}$  values and a decrease in corresponding  $d_p$ . However, no repeatable pattern has been derived from the pore size analysis and  $S_{BET}$  estimation.

By combining the results of particle size and pore size distribution analysis, it can be deduced that upon sonication of P25 suspension, external surface area,  $S_v$ , decreases when particles aggregate. Simultaneously, corresponding  $S_{BET}$  and  $d_p$  values increased. On the other hand, when PC105 is exposed to ultrasound, smaller particles can be obtained while both  $S_{BET}$  and  $S_v$  increased. The observed decrease in  $d_p$  (PC105) and the difference in the porosity of P25 and PC105 upon exposure to ultrasound, offer an evidence for the anatase instability towards ultrasound. Since P25 is composed of 25% of rutile, the fact that its porosity seems to be more preserved during sonication prove the postulated theory of anatase instability. Moreover, even the observed irregular aggregation of TiO<sub>2</sub> particles can be justified; during sonication with low frequency ultrasound, cavitation in water is evident causing a formation of free radicals and H<sub>2</sub>O<sub>2</sub> [26, 27] even in the absence of solid particles. Those species can serve as a bridge for further aggregation of TiO<sub>2</sub> particles. In that manner, a certain aggregation of TiO<sub>2</sub> is expected and does not indicate its instability.

### Preliminary kinetic study

A generally adopted mechanism for the heterogeneous photocatalysis of the most of organic compounds is the Langmuir–Hinshelwood (L–H) mechanism for surface catalysis. The L–H mechanism suggest that reaction occurs between species that are

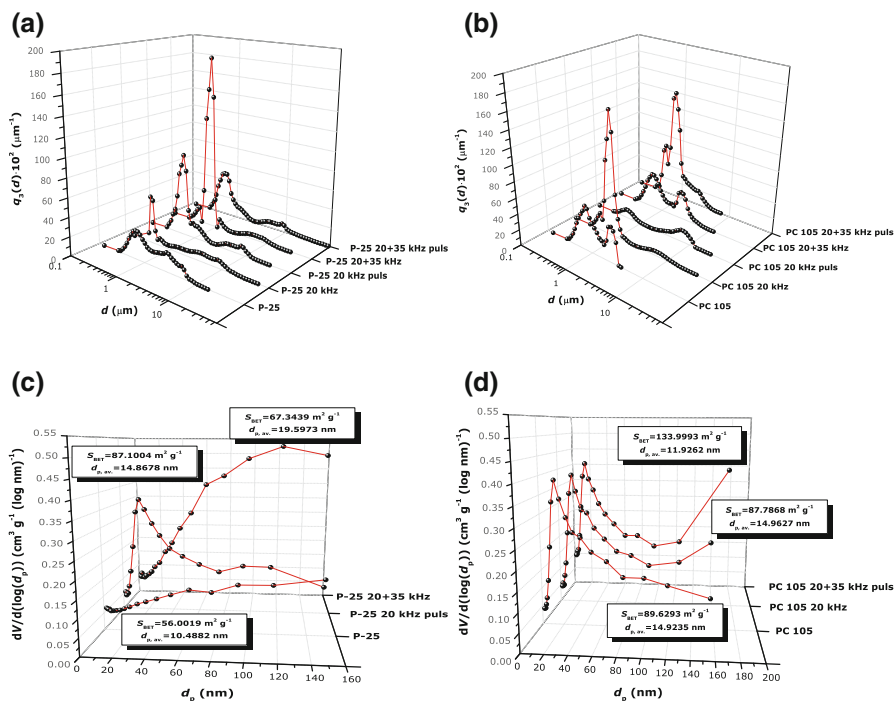


**Fig. 3** Experimental size distribution data for: **a** particles of TiO<sub>2</sub> P-25, **b** particles of TiO<sub>2</sub> PC105, **c** pores of TiO<sub>2</sub> P-25 and **d** pores of TiO<sub>2</sub> PC105 sample after 20 min of sonication

adsorbed on the surface, by assuming the adsorption and a consecutive reaction with the reactive species (radicals, holes) on the catalysts surface [21]. In that manner, L–H mechanism is assumed also for the sonocatalysis studied in this work.

Previous studies of photocatalytic degradation kinetics of organic pollutants indicated that the destruction rates of photocatalytic oxidation of various dyes over illuminated TiO<sub>2</sub> obeyed the L–H kinetics model [20, 22, 28]. However, when the initial chemical concentration of pollutant, e.g. dye ([dye]<sub>0</sub>) is a millimolar solution, the equation can be simplified to an apparent first-order equation, Eq. 3;

$$[\text{dye}]_t = [\text{dye}]_0 \exp^{-kt} \tag{3}$$

A plot of  $\ln([\text{dye}]_t/[\text{dye}]_0)$  versus time represents a straight line, the slope of which upon linear regression equals the apparent first order rate constant *k*. Generally, first order kinetics is appropriate for the entire concentration range up to few ppm. Several studies were reasonably well fitted by this kinetic model [28–31].

The rate equations (Eq. 4) used in the present models for photocatalysis and sonocatalysis referred to dye and oxalic acid degradation were derived by considering the following:

1. The rates of catalytic oxidation of organic substrates can often be fitted by a L–H rate equation and their initial concentration is low, thus the L–H rate equation reduces to a first order kinetic rate equation (*n* = 1).

2. The reaction mechanism can be based on both surface reaction with holes,  $h^+$  and hydroxyl radicals,  $\cdot OH$ ; the kinetic rate constant follows a power law expression and the exponent in the absence of mass transfer limitations varies between 0.5 and 1. Raw kinetic data can be fitted according to square root dependence ( $n = 0.5$ ).

$$r_j = -k_j[\text{pollutant}]^n \quad (4)$$

The equation will be further used to express the mineralization kinetics, Eq. 5:

$$r_{\text{TOC}} = -k_{\text{TOC}}[\text{OC}]^n \quad (5)$$

where  $j$  denotes the studied pollutant, and (OC) denote the molar concentration of organic content in the system (TOC/12).

The two group of model compound chosen: aliphatic (oxalic acid) and aromatic (azo dyes) differ in the incident light absorption properties and the complexity of their degradation mechanisms [6, 26]. Accordingly, a comparison of their degradation behavior allowed us to address the role of the presented mechanistic aspects on the degradation kinetics.

The degradation kinetics of the studied pollutants and model solutions is presented in Figs. 4, 5 and 6. The observed trend of mineralization and dye degradation indicate a reaction order different from zero. To clarify the preferred degradation mechanism of the studied organic compounds, kinetic data were fitted with both half-order and first order kinetic models applied to a batch reactor mass equation as a preliminary step. From the obtained results (Figs. 4, 5, 6), it is evident that both kinetic models describe the mineralization and degradation kinetics of oxalic acid, RV2 and certain mixtures, suggesting that these pollutants could simultaneously undergo both fast reaction with  $\cdot OH$  radicals ( $n = 1$ ) and slow hole trapping mechanism ( $n = 0.5$ ). In the case of UV-C photocatalysis, both models are adequate to describe the MY10 degradation kinetics. It needs to be clarified that the concentration of oxalic acid was monitored by TOC measurements and HPLC analysis, simultaneously. HPLC analysis was performed to exclude the oxalic acid degradation route through formic acid [22]. In the first 10 min, the generation of a small portion of formic acid was observed; maximally 7.3 % of the corresponding TOC value (results not shown). It was further noticed that both acids are readily decomposed and their concentration decreases in time (according to HPLC analysis). The obtained TOC values correspond mainly with the concentration of oxalic acid. Thus, a generation of formic acid can be neglected.

The differences were observed during the application of different type of UV irradiation, i.e. photocatalytic treatment of model wastewaters resulted in various mineralization extents depending on the type of irradiation used (Fig. 7). The photocatalytic efficiency appeared to be influenced by the presence of dye molecules; especially by the presence of MY10 (DAW2, DAW3). Molecules of MY10 absorb a significant portion of useful irradiation; below 380 nm (Table 1). The absorption maximum for MY10 is at 365 nm, with a broad peak over 400 nm. This filtering effect of MY10 was also recognized during the kinetic study; the degradation of MY10 and corresponding mixtures cannot be described by the applied kinetic models in the entire time span (Fig. 6). MY10 molecules and  $TiO_2$

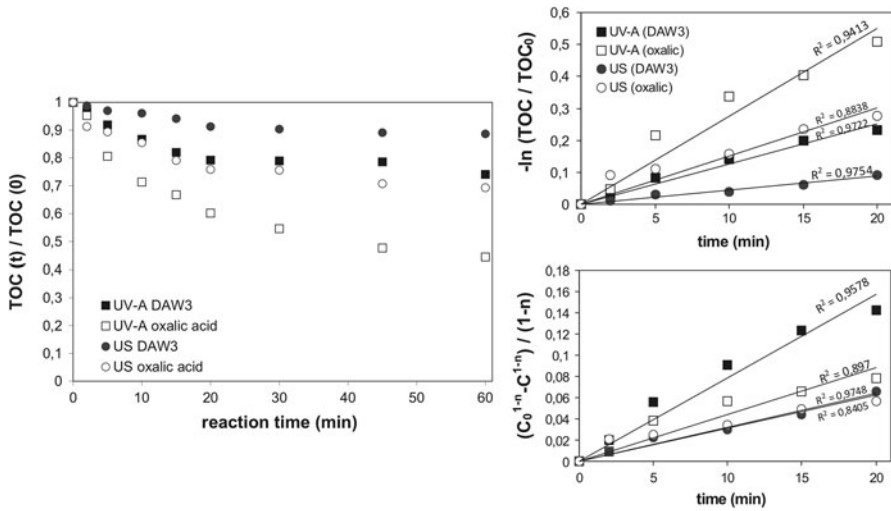


**Fig. 4** Mineralization kinetics for oxalic acid model solution and DAW mixture using PC-500 (raw powder in photocatalysis and calcined sample in sonocatalysis); fit with first and half-order kinetic models

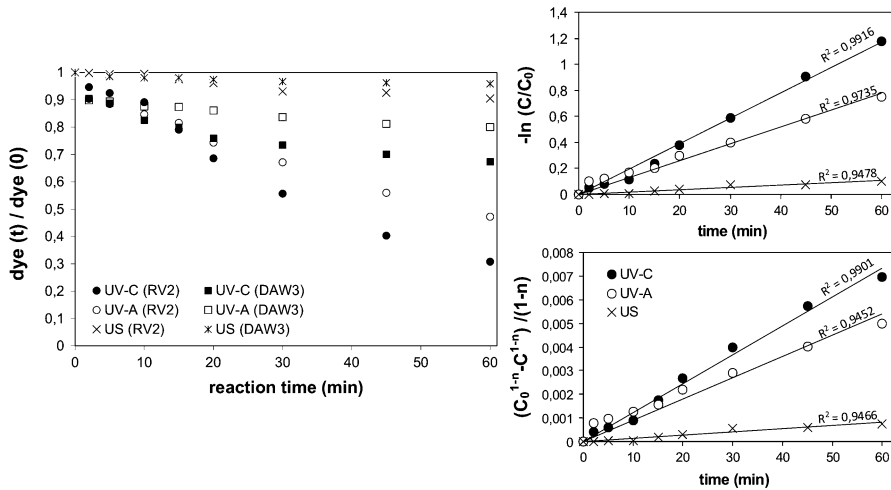


**Fig. 5** Kinetic study for degradation of RV2 in single compound model solution (RV2) and DAW3 mixture by applied processes using PC-500

compete for the quantum of incident irradiation reaching catalysts surface, whose intensity is already reduced due to the absorption of certain portion of light in the semi-transparent bulk solution. Assuming the continuous adsorption of MY10 on the catalyst surface, degradation process slows down until it is stopped.

The related preliminary kinetic study showed that in the case of sonocatalysis, phenomena similar to photocatalysis can be observed. The kinetic data from sonocatalytic experiments can be fitted well by the applied half-order and first order

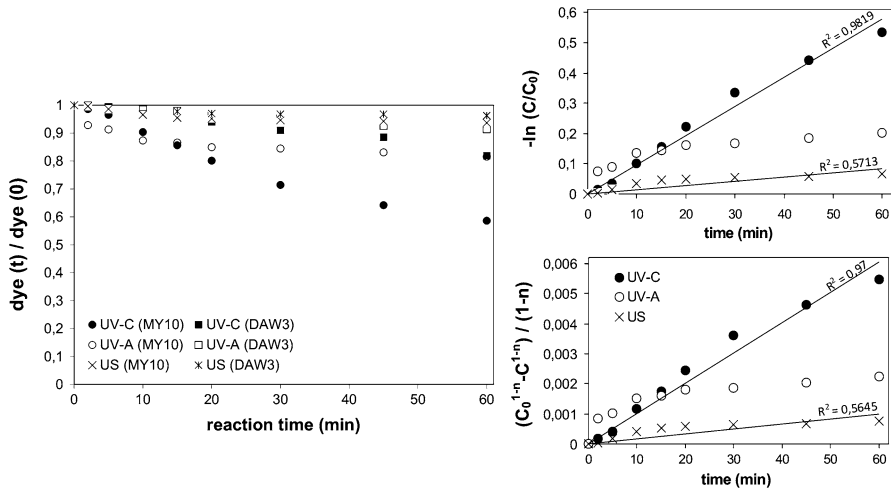


**Fig. 6** Kinetic study for degradation of MY10 in single compound model solution (MY10) and DAW3 mixture by applied processes using PC-500

kinetic models. I.e. in sonocatalysis, the reaction between pollutants and ·OH radicals occurs parallel with the reaction between generated  $h^+$  on the catalysts surface and the adsorbed pollutant. Moreover, in the case of MY10 sonocatalysis, both kinetic models are inadequate in the entire time span and the trend is quite similar to the one observed during UV-A photocatalysis. The latter favors the theory of sonoluminescence and the excitation of  $TiO_2$  by the light emitted upon bubble/cavity collapse. Throughout the course of bubble collapse, the kinetic energy of species within the bubble increases, leading to inelastic collisions; water molecules can be excited in various states upon collisions and radicals are formed. Radicals can be

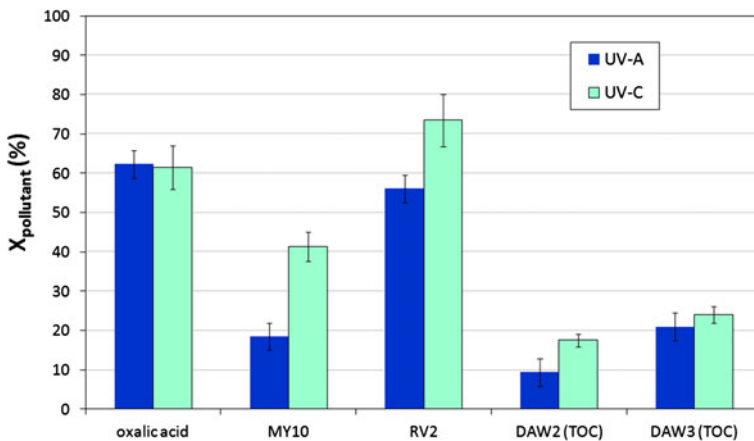


**Fig. 7** Mineralization extents achieved after 60 min of photocatalytic degradation of pollutants in different model solutions by PC-500 in respect to type of applied irradiation

further excited by collisions to give an emission of light. In general, the spectra of water sonoluminesce consist of emission from ·OH radicals (280–340 nm) and a continuum of uncertain origin ( $\lambda_{\text{max}} = 425 \text{ nm}$ ) [32].

The competition of pollutants (dye, oxalic acid) in the mixture to access the active centers of catalysts is noted. The observed degradation of MY10 and RV2 is faster in the case of single dye solutions than in mixtures (e.g. DAW3 as presented in Figs. 5a, 6a). After 60 min of applied UV-C photocatalysis, 73 % of RV2 is decomposed in RV2 model solution and only 33 % in DAW3 mixture. Likewise, 41 % of MY10 is decomposed in MY10 solution and 19 % in DAW3. Despite results for UV-A photocatalysis of MY10, the efficiency of UV-C photocatalysis is quite low in comparison to results obtained for RV2. The underlying reason might be found in dye molecule shape and size. Namely, MY10 is a small molecule that consists of only two benzene rings (Table 1). In contrast to larger RV2 molecules, MY10 can better reach the catalysts surface and accumulate near surface, causing the reduction of irradiation intensity on unoccupied catalyst surface.

### Detailed kinetic study

The mineralization of organic content toward  $\text{CO}_2$  was chosen as a comparable overall reaction that occurs in all the investigated systems. This overall reaction represents a series of step reactions (or elementary processes), since a complete certainty of the steps is not possible, especially taking into account a variety of short-lived species (e.g., ·OH) and intermediates. Therefore, based on literature data, half and first order kinetics were chosen to define the slowest rate determining step during the time span. The preliminary results pointed to the two simultaneous kinetic pathways. However, the fitting of experimental data by both expressions merely served as a base for further kinetic considerations. As reported by Pozzo et al. [22], the photodegradation of oxalic acid proceeds by both mechanisms as discussed. In addition, oxalic acid and the  $\text{TiO}_2$  surface forms two types of complexes: stable and labile. Oxalate ions linked via more labile complex reacts with generated ·OH radicals, while the oxalate ions linked via stable complexes degrades slowly due to  $\text{h}^+$  trapping. The surface coverage by these complexes changes during the reaction; labile ones are readily degraded by ·OH radicals, leaving the available sites for the formation of stable complexes on the  $\text{TiO}_2$  surface. These considerations can be written as follows, Eq. 6:

$$r_{\text{oxalic}} = k_1 \theta(t) [\text{oxalic} (t)] + k_{0.5}(1 - \theta(t)) ([\text{oxalic} (t)])^{0.5} \quad (6)$$

where  $k_1$  and  $k_{0.5}$  represent the apparent rate constant for the reaction of the oxalate ions with ·OH radicals and holes, respectively, while  $\theta(t)$  represents the surface coverage by labile complex. Note that the sum of surface coverage by both complexes is 1, relating to the assumption that hydroxyl groups and oxygen occupy sites different than the pollutant [22]. The given equation differs from the one given by Pozzo et al. [22] only in one issue: the square root dependence of overall reaction rate ( $r_{\text{oxalic}}$ ) on the volumetric rate of photon absorption in the reaction space ( $e_a$ ). In the case when  $e_a$  is introduced into the kinetic model, intrinsic reaction rate

constants are obtained. Nevertheless, in the present study, only apparent rates are observed.

Furthermore, the surface coverage during reaction is determined by the following expression, Eq. 7:

$$\theta(t) = \mathbf{a}[\text{oxalic}(t=0)](1 - \mathbf{b}t) \quad (7)$$

This equation is also quite similar to the reported one [22]. Note that coefficient **b** includes  $e_a$ . The volumetric rate of photon absorption depends on the irradiation type, irradiance, reactor geometry and optical properties of the photocatalysts ([22] and references therein).

Since other studied pollutants (dyes) showed a behavior similar to oxalic acid during the preliminary kinetic study, it was assumed that dyes RV2 and MY10 link to the  $\text{TiO}_2$  surface via stable and labile complexes. Having in mind the complex structure of RV2, it is reasonable to conclude that in case of RV2, there is no single stable or labile complex but variety of different complexes that can be grouped into either stable or labile group of complexes. These observations are summed up in the following expressions, Eqs. 8 and 9:

$$r_{\text{dye}} = k_1 \theta_{\text{dye}}(t) [\text{dye}(t)] + k_{0.5} (1 - \theta_{\text{dye}}(t)) ([\text{dye}(t)])^{0.5} \quad (8)$$

$$\theta_{\text{dye}}(t) = \mathbf{a}[\text{dye}(t=0)](1 - \mathbf{b}t) \quad (9)$$

It can be even more generalized, and one can say that majority of organic molecules can form stable and labile complexes with  $\text{TiO}_2$  surface, resulting in the two simultaneous reaction pathways, i.e. degradation via  $\cdot\text{OH}$  radicals and  $h^+$ , Eqs. 10 and 11.

$$r_{\text{OC}} = k_1 \theta_{\text{OC}}(t) [\text{OC}(t)] + k_{0.5} (1 - \theta_{\text{OC}}(t)) ([\text{OC}(t)])^{0.5} \quad (10)$$

$$\theta_{\text{OC}}(t) = \mathbf{a}[\text{OC}(t=0)](1 - \mathbf{b}t) \quad (11)$$

In these equations,  $k_1$  and  $k_{0.5}$  represent the apparent rate constant for the reaction between organic matter (OC) and  $\cdot\text{OH}$  radicals and holes, respectively, while  $\theta_{\text{OC}}(t)$  represents the surface coverage by labile group of complexes. Coefficients **a** and **b** are fitted in models. Coefficient **a** was adjusted to  $\theta(t=0) = 0.7$  in all systems.

Results of such kinetic modeling are given in Fig. 8a–c. The model follows the trend of experimental data in all cases of the oxalic acid oxidation, mineralization of DAW3 and RV2 decolorization by applying UV-C and UV-A light and acoustic cavitation. The corresponding reaction rate constants,  $k_1$  and  $k_{0.5}$ , and coefficients **a** and **b** are given in Table 4. These parameters are determined using the finite difference method for solving of the rate equations, with the step:  $\Delta t = 1\text{s}$ .

Furthermore, the effect of the irradiance level is taken into account. Namely, observed apparent reaction rate constants differ for the same factor when different type of irradiation was applied. The observed rate constants are products of intrinsic rate constants and a square root of volumetric rate of photon absorption,  $e_a$ . It is simplified to Eq. 12:



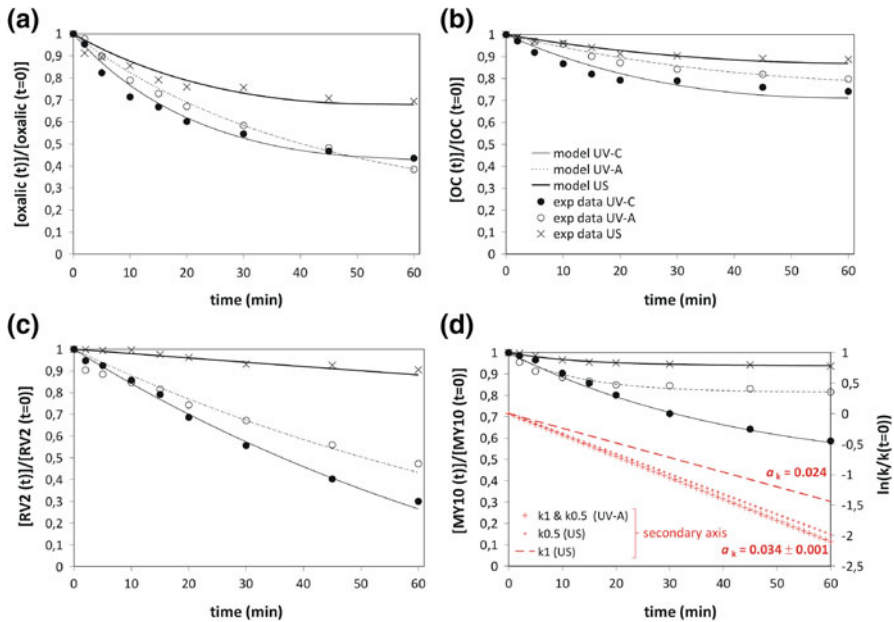


**Fig. 8** Results of detailed kinetic study for **a** oxalic acid oxidation, **b** DAW3 mineralization, **c** RV2 decolorization and **d** MY10 decolorization by applied processes using PC-500 (legend shown in (b); additional legend in (d))

$$k_1/k_{1,intrinsic} = k_{0.5}/k_{0.5,intrinsic} = (e_a)^{0.5} \tag{12}$$

In the same manner, coefficient **b** is a product of “intrinsic” **b** and  $e_a$  [22].

Finally, photocatalysis by UV-C and UV-A light and sonocatalysis can be compared in Eqs. 13 and 14.

$$k_{1(UV-C)}/k_{1(UV-A)} = k_{0.5(UV-C)}/k_{0.5(UV-A)} = (\mathbf{b}_{(UV-C)}/\mathbf{b}_{(UV-A)})^{0.5} = Z_1 \tag{13}$$

$$\begin{aligned} k_{1(UV-C)}/k_{1(sonoluminescence)} &= k_{0.5(UV-C)}/k_{0.5(sonoluminescence)} \\ &= (\mathbf{b}_{(UV-C)}/\mathbf{b}_{(sonoluminescence)})^{0.5} = Z_2 \end{aligned} \tag{14}$$

By finding the ratios  $Z_1$  and  $Z_2$  we can validate the model and confirm the thorough kinetic considerations. Results are given in Table 4, showing the match between these ratios obtained from different experiments. Interestingly, the ratio of  $k_{1(UV-C)}$  and  $k_{1(sonoluminescence)}$  is slightly lower than  $Z_2$ , which can be explained by the generation of additional portion of  $\cdot\text{OH}$  radicals due to acoustic cavitation of bulk solution. Also, ratio between  $\mathbf{b}_{(UV-C)}$  and  $\mathbf{b}_{(sonoluminescence)}$  is lower than  $Z_2^2$ . The possible explanation is that ultrasound contributes the higher surface coverage by stable complexes. Ratios  $Z_1$  and  $Z_2$  for dyes and DAW3 mixture differ from the ones observed for oxalic acid. This observation favors the assumption that dyes behave as filters for UV-A irradiation. As shown in Table 4, determined  $Z_1$  and  $Z_2$  for RV2 are slightly lower than the ones obtained for oxalic acid, while  $Z_1$  and  $Z_2$

**Table 4** Evaluation of the detailed kinetic study: estimated reaction rate constants and model coefficients

Term	<b>a</b>		$Z_1$	$Z_2$	UV-C		UV-A		US			
	$60 k_1$ , ( $s^{-1}$ )	$60 k_{0.5}$ , ( $mol^{0.5} dm^{1.5} s^{-1}$ )			<b>b</b>	$60 k_1$ , ( $s^{-1}$ )	$60 k_{0.5}$ , ( $mol^{0.5} dm^{1.5} s^{-1}$ )	<b>b</b>	$60 k_1$ , ( $s^{-1}$ )	$60 k_{0.5}$ , ( $mol^{0.5} dm^{1.5} s^{-1}$ )	<b>b</b>	
Oxalic acid	950	0.72	0.20	0.033	$6.6 \times 10^{-5}$	0.020	0.024	$4.7 \times 10^{-5}$	0.010	0.017	$1.3 \times 10^{-5}$	0.015
DAW3 (TOC)	230	0.42	0.12	0.016	$3.9 \times 10^{-5}$	0.018	0.0067	$1.6 \times 10^{-5}$	0.012	0.0037	$2.2 \times 10^{-6}$	0.010
RV2	9,960	0.63	0.17	0.023	$9.7 \times 10^{-5}$	0.019	0.0145	$6.1 \times 10^{-5}$	0.007	0.0059	$1.6 \times 10^{-5}$	0.018
MY10 <sup>a</sup>	5,100	0.47	0.13	0.017	$4.5 \times 10^{-5}$	0.018	0.0089	$2.1 \times 10^{-5}$	0.007	0.0041	$5.8 \times 10^{-6}$	0.013

<sup>a</sup> Values defined in  $t = 0$

for DAW3 and MY10 are almost twice lower. The latter correspond with the dyes ability to absorb the light at  $\lambda = 365$  nm (extinction coefficient given in Table 1).

Finally, a filtering effect of MY10 was explored. As given in Fig. 8d, experimental data for MY10 degradation can be fitted by the presented kinetic model (Eq. 8) if the corresponding reaction rate constants vary during the time span. Since the observed apparent constants are the product of the intrinsic constant and the volumetric rate of photon absorption by the photocatalyst ( $\text{TiO}_2$ ), if the photon absorption by  $\text{TiO}_2$  change through time, constants  $k_1$  and  $k_{0.5}$  can change accordingly.

As shown in Fig. 8d, an exponential decay of both rate constant was observed with the corresponding decay coefficient  $a_k$ . The equality of decay coefficients ( $0.033\text{--}0.035\text{ s}^{-1}$ ) favors the validity of the established assumptions. Namely, it can be concluded that  $k_1$  and  $k_{0.5}$  decreased exponentially as photon absorption by  $\text{TiO}_2$  decreased due to irradiation filtering by MY10. In the case of sonocatalysis, a decay coefficient  $a_k$  for  $k_1$  is lower ( $0.024\text{ s}^{-1}$ ). This observation can be again explained by the generation of  $\cdot\text{OH}$  radicals in bulk solution due to acoustic cavitation. In sonocatalysis, both effects of acoustic cavitation and sonoluminescence are responsible for pollutant degradation. Sonoluminescence affects the generation of hole-electron pairs on  $\text{TiO}_2$  surface, while the acoustic cavitation in bulk results with the additional portion of  $\cdot\text{OH}$  radicals.

## Conclusions

With the purpose of potential application in the treatment of colored wastewater, photocatalytic and sonocatalytic processes with the introduction of different types of commercial and calcined  $\text{TiO}_2$  were studied.

Commercial  $\text{TiO}_2$  catalyst (mostly anatase) was found to be more efficient in photocatalytic process of model pollutants degradation. The calcined  $\text{TiO}_2$  catalyst with confirmed rutile form, was found to be more efficient in sonocatalytic process of model pollutants degradation and mineralization. According to the characterization of granulometric properties under certain conditions, anatase-like  $\text{TiO}_2$  appeared as unstable in ultrasound.

Preliminary studies on the degradation and mineralization kinetics of dyes RV2, MY10, oxalic acid and their mixtures showed that raw kinetic data fit well ( $R^2 > 0.94$ ) into the half and first order reaction rate model, pointing at the two ongoing mechanisms, i.e. reaction with  $\cdot\text{OH}$  radicals and direct electron transfer between adsorbed molecules and catalyst surface. The performed study confirmed the similarity of occurring mechanisms in photocatalysis and sonocatalysis. Moreover, the results indicate the validity of sonoluminescence theory; MY10 ( $\lambda_{\text{max}} = 365$  nm) influenced the sonocatalytic efficiency drastically. According to the sonoluminescence theory, the emitted light upon bubble collapse is responsible for the excitation of  $\text{TiO}_2$ .

The detailed kinetic analysis (inspired by [22]) confirmed the two simultaneous kinetic pathways, and the similarity of photocatalytic mechanism for all the studied pollutants. In sonocatalysis, both acoustic cavitation and sonoluminescence affect

the pollutant degradation; excitation of sonoluminescence affect  $\text{TiO}_2$  by sonoluminescence is measurable through the apparent reaction rate constants, while an additional portion of  $\cdot\text{OH}$  radicals generated upon the acoustic cavitation causes an increase of constant  $k_1$  above an expected level.

The highest decolorization and mineralization extents of MY10 and RV2 were achieved by photocatalysis using UV-C irradiation and anatase  $\text{TiO}_2$  (PC105).

**Acknowledgments** The authors would like to acknowledge the financial support from the COGITO bilateral project Air and water pollutants abatement on mesoporous silicates modified by oxide particles using advanced oxidation technologies (prof. Vesna Tomašić). The authors would also like to thank prof. Anne Davidson, UPMC, France for complementary analyses.

## References

1. Arslan Alaton I, Balcioglu IA, Bahnemann DW (2002) *Water Res* 36:1143–1154
2. Pekakis PA, Xekoukoulotakis NP, Mantzavinou D (2006) *Water Res* 40:1276–1286
3. Konstantinou IK, Albanis TA (2004) *Appl Catal B Environ* 49:1–14
4. Grčić I, Papić S, Koprivanac N, Kovačić I (2012) *Water Res* 46:5683–5695
5. Grčić I (2011) Modelling of the photocatalytic and sonochemical process for the wastewater treatment. Ph.D. dissertation, University of Zagreb
6. Grčić I, Vujević D, Koprivanac N (2010) *Chem Eng J* 157:35–44
7. Beltran FJ (2003) In: Tarr MA (ed) *Chemical degradation methods for wastes and pollutants—environmental and industrial applications*. Marcel Dekker Inc., New York, pp 1–77
8. Herrmann J-M (1999) *Catal Today* 53:115–129
9. Mills A, Lee S-K (2004) In: Parsons S (ed) *Advanced oxidation processes for water and wastewater treatment*. IWA Publishing, Cornwall, pp 137–167
10. Han F, Kambala VSR, Srinivasan M, Rajarathnam D, Naidu R (2009) *Appl Catal A Gen* 359:25–40
11. Wang J, Jiang Z, Zhang L, Kang P, Xie Y, Lv Y, Xu R, Zhang X (2009) *Ultrason Sonochem* 16:225–231
12. Eren Z, Ince NH (2010) *J Hazard Mater* 177:1019–1024
13. Kim JK, Martinez F, Metcalfe IS (2007) *Catal Today* 124:224–231
14. Shimizu N, Ogino C, Dadjour MF (2007) *Ultrason Sonochem* 14:184–190
15. Wang J, Jiang Z, Zhang Z, Zhao G, Zhang G, Ma T, Sun W (2007) *Desalination* 216:196–208
16. Pang YL, Abdullah AZ, Bhatia S (2011) *Chem Eng J* 166:873–880
17. Pang YL, Abdullah AZ (2012) *Ultrason Sonochem* 19:642–651
18. Wang J, Guo B, Zhang X, Zhang Z, Han J, Wu J (2005) *Ultrason Sonochem* 12:331–337
19. Ogi H, Hirao M, Shimoyama M (2002) *Ultrasonics* 40:649–650
20. Bahnemann D, Hilgendorff M, Memming R (1997) *J Phys Chem* 101:4265–4275
21. Krýsa J, Waldner G, Měšťánková H, Jirkovsky J, Grabner G (2006) *Appl Catal B Environ* 64:290–301
22. Pozzo RL, Brandi RJ, Cassano AE, Baltanás MA (2010) *Chem Eng Sci* 65:1345–1353
23. Wang J, Ma T, Zhang Z, Zhang X, Jiang Y, Zhang G, Zhao G, Zhao H, Zhang P (2007) *Ultrason Sonochem* 14:246–252
24. Grčić I, Koprivanac N, Vujević D, Papić S (2008) *J Adv Oxid Technol* 11:91–96
25. Grčić I, Vujević D, Koprivanac N (2010) *Chem Biochem Eng Q* 24:387–400
26. Grčić I, Obradović M, Vujević D, Koprivanac N (2010) *Chem Eng J* 164:196–207
27. Her N, Park J-S, Yoon Y (2011) *Chem Eng J* 166:184–190
28. McMurray TA, Byrne JA, Dunlop PSM, Winkelmann JGM, Eggins BR, McAdams ET (2004) *Appl Catal A Gen* 262:105–110
29. Kosanić MM (1998) *J Photochem Photobiol A Chem* 119:119–122
30. Guettaï N, Ait Amar H (2005) *Desalination* 185:439–448
31. Kumar J, Bansal A (2012) *Int J Environ Sci Technol* 9:479–484
32. Didenko YT, McNamara WB III, Suslick KS (1999) *J Phys Chem A* 103:10783–10788